Environmental Technology & Innovation 32 (2023) 103273

Contents lists available at ScienceDirect

Environmental Technology & Innovation

journal homepage: www.elsevier.com/locate/eti

Oxidative degradation of polyethylene by two novel laccase-like multicopper oxidases from *Rhodococcus opacus* R7.

Jessica Zampolli [a], Marco Mangiagalli [a], Daniele Vezzini [a], Marina Lasagni [b], Diletta Ami [a], Antonino Natalello [a], Federica Arrigoni [a], Luca Bertini [a], Marina Lotti [a], Patrizia Di Gennaro [a,*]

[a] *Department of Biotechnology and Biosciences, University of Milano-Bicocca, Piazza della Scienza 2, 20126 Milan, Italy*
[b] *Department of Earth and Environmental Sciences, University of Milano-Bicocca, Piazza della Scienza 1, 20126 Milan, Italy*

ARTICLE INFO

Article history:
Received 12 April 2023
Received in revised form 28 June 2023
Accepted 30 June 2023
Available online 7 July 2023

Keywords:
Polyethylene
Biodegradation
Rhodococcus genus
Plastic waste
Laccase-like enzyme
Multicopper oxidase

ABSTRACT

The production of synthetic plastics, especially polyethylene, has reached a crucial level, making highly challenging plastic waste management. This paper aims to elucidate the role of two novel laccase-like multicopper oxidases in polyethylene oxidative degradation based on transcriptomic data from *Rhodococcus opacus* R7 grown on polyethylene. The purification of the recombinant proteins, LMCO2 and LMCO3 belonging respectively to the three- and two-domains laccase families, showed that they are endowed with different functional features. LMCO2 showed the highest enzyme activity at 65 °C with an optimal pH of 7.0, while LMCO3 exhibited the highest activity at 80 °C at acidic pH. LMCOs showed activity on both phenolic (*i.e.*, 2,6-DMP) and non-phenolic (*i.e.*, ABTS) compounds and they were thermostable.

The oxidative activity of LMCO2 and LMCO3 on untreated low-density polyethylene was assessed by combining Fourier transform infrared spectroscopy and gas chromatography coupled with mass spectrometry analyses. Oxidation of PE was recorded within a short time range (24-48 h) and revealed previously not described patterns of alkyl compounds and oxygenated products including ketones, alcohols, and carboxylic acids. Structural analysis of LMCO2 and LMCO3 together with density functional theory calculations allowed to identify structural and electronic elements presumably involved in the oxidation of polyethylene.

1. Introduction

Since synthetic plastic has gained a crucial role for diverse purposes, managing plastic pollution has become a critical challenge due to ever-increasing post-consumer plastic waste (Yeung et al., 2021).

Among petroleum-based plastic, polyethylene (PE) is one of the most produced and utilized polyolefins because of its remarkable features of robustness, low cost of production, and flexibility (Plastics Europe, 2019). PE is a carbon–carbon (C-C) backbone thermoplastic deriving from the polymerization process of ethylene monomers. The accumulation of PE raises

* Correspondence to: University of Milano-Bicocca, Piazza della Scienza 2, 20126 Milan, Italy.
E-mail addresses: jessica.zampolli@unimib.it (J. Zampolli), marco.mangiagalli@unimib.it (M. Mangiagalli), daniele.vezzini@unimib.it (D. Vezzini), marina.lasagni@unimib.it (M. Lasagni), diletta.ami@unimib.it (D. Ami), antonino.natalello@unimib.it (A. Natalello), federica.arrigoni@unimib.it (F. Arrigoni), luca.bertini@unimib.it (L. Bertini), marina.lotti@unimib.it (M. Lotti), patrizia.digennaro@unimib.it (P. Di Gennaro).

https://doi.org/10.1016/j.eti.2023.103273

major concerns because of its long half-life and high persistence in the environment (Yeung et al., 2021). Different fates can be faced by PE polymers after their useful end-of-life (Andler et al., 2022), including recycling and/or biodegradation processes involving microorganisms, or their enzymes (Andler et al., 2022; Zhang et al., 2021). Currently, the microbial biodegradation of plastics is receiving substantial attention to mitigate the plastic pollution issue (Andler et al., 2022). However, C–C backbone plastic is recalcitrant to biodegradation due to the lack of hydrolyzable groups. To date, the microbial degradation of C–C backbone plastic has not been fully understood and exploited, and little is known about the metabolic pathways, the involved enzymes, and the mechanisms of PE biodegradation (Restrepo-Flórez et al., 2014; Andler et al., 2022; Zhang et al., 2022b). Literature reports only show that the first PE oxidation generates shorter aliphatic fragments that can be further degraded by subsequent oxidation steps (Pathak and Navneet, 2017).

Besides fungal genera with notable PE-degrading ability, a few bacterial genera have been characterized for their PE biodegradative abilities (Montazer et al., 2019, 2020; Zhang et al., 2022b; Cowan et al., 2022); bacteria of *Rhodococcus* genus are of primary interest for their extraordinary metabolic capabilities and the considerable potential in plastic degradation as shown by Zampolli et al.(Zampolli et al., 2022). Among them, *R. ruber* C208 can biodegrade UV-pretreated PE under the activation of alkane degradation and β-oxidation of fatty acid pathways (Santo et al., 2013; Gravouil et al., 2017). *R. opacus* R7 grown on untreated PE as the only carbon and energy source activates genes encoding extracellular laccase-like multicopper oxidases (LMCOs) (Zampolli et al., 2021). Furthermore, the transcription of multiple R7 oxidoreductases including a monooxygenase (*alkB*), a cytochrome P450 hydroxylase (*cyp450*), and genes encoding putative membrane transporters were up-regulated (Zampolli et al., 2021). Another interesting feature of *R. opacus* R7 is its ability to grow on and biodegrade medium-chain *n*-alkanes and carboxylic acids with different chain lengths (Zampolli et al., 2014, 2020).

The production of suited enzymes for biocatalytic degradation and/or biotransformation seems a promising route for sustainable PE-based plastic depolymerization to accompany plastic recycling (Amobonye et al., 2021). The most reported enzymes likely known for PE depolymerization include laccases (EC 1.10.3.2), manganese peroxidases (EC 1.11.1.13), and lignin peroxidases (EC 1.11.1.14) (Pometto et al., 1992; Fujisawa et al., 2001; Santo et al., 2013; Sowmya et al., 2015; Wei and Zimmermann, 2017; Yao et al., 2022), as suggested by experimental evidence obtained either using PE UV-irradiated or heat-treated (Santo et al., 2013; Sowmya et al., 2014, 2015) or using laccase-mediator systems (LMSs) (Pometto et al., 1992; Fujisawa et al., 2001; Yao et al., 2022; Zhang et al., 2022b). Among laccases, a few LMCOs are reported as PE-degrading enzymes, recognizable based on the cupredoxin-like domain number which displays the typical Greek key β-barrel fold. The two-domain (2dLMCO) generally presents a trimeric quaternary structure, whilst the three-domain (3dLMCO) a monomeric one (Gräff et al., 2020). The active site of these enzymes consists of a type 1 (T1) copper site where the substrate is oxidized, and a trinuclear copper cluster (T2 and T3) where the oxygen is activated and reduced. It is well established that laccases are promiscuous enzymes able to perform 1e oxidation of various substrates ranging from phenolic to non-phenolic compounds related to lignin as well as some aliphatic polymers and (polycyclic) aromatic hydrocarbons (Jones and Solomon, 2015).

Although a few studies showed enzymatic oxidation of PE by direct enzymatic catalysis in the supernatant of PE-degrading bacteria (Pometto et al., 1992; Fujisawa et al., 2001; Santo et al., 2013; Sowmya et al., 2014, 2015; Yao et al., 2022; Zampolli et al., 2021), knowledge about the mechanism of PE enzymatic oxidation is still vague.

The aim of this paper is the characterization and the activity of two novel extracellular LMCOs from *R. opacus* R7 selected on the basis of previous transcriptomic data (Zampolli et al., 2021) in order to comprehend their role in the PE biodegradative pathway. The recombinant production of LMCO2 and LMCO3 enabled the subsequent in-depth biochemical and biophysical characterization. Their oxidative activity on untreated low-density PE was assessed by two orthogonal techniques such as Fourier transform infrared (FTIR) spectroscopy and gas chromatography coupled with mass spectrometry (GC-MSD) analyses. Finally, LMCO2 and LMCO3 structural predictions, together with density functional theory (DFT) calculations, provided hints about the structural and electronic features that may play a role in the PE oxidation mechanism.

2. Materials and methods

2.1. Bacterial strains and growth conditions

Bacterial strains and plasmids used in this study are listed in Table S1. Growth maintenance conditions for *Escherichia coli* DH5α and *Rhodococcus erythropolis* AP (CIP 110799) are described in (Zampolli et al., 2014). Wild type and the recombinant strains of *R. erythropolis* AP were cultivated on M9 mineral medium (Maniatis et al., 1982) added with 20 mM malate (156 mg L^{-1}).

To obtain the competent cells, after pre-cultured *R. erythropolis* AP on Luria-Bertani medium (LB) at 30 °C, AP strain was grown on 100 mL LB medium amended with 1.5% glycine (stock *w/v*, 10%) and 1.8% sucrose (stock *w/v*, 36%) at an initial optical density at 600 nm (OD_{600}) of 0.05 at 30 °C (160 rpm). Standard molecular techniques were applied for DNA manipulation, enzymatic digests, ligation, and PCR reactions (Sambrook and Russell, 1989).

2.2. Bioinformatics analysis of LMCO2 and LMCO3 from R. opacus R7

R. opacus R7 genes for recombinant strain generation and subsequent enzyme production were selected based on transcriptomic results after R7 growth on untreated powder PE (Zampolli et al., 2021). Sequence analysis and multiple sequence alignments of LMCO2 (AII11185) and LMCO3 (AII11221) were carried out by using the BLASTn tool (Altschul et al., 1990) of NCBI pipeline, Clustal Omega (Thompson et al., 1994) and InterPro (Mitchell et al., 2019).

2.3. R. opacus R7 LMCOs cloning

The genes coding for laccase-like multicopper oxidase (*LMCO2* and *LMCO3*) deleted of the conserved twin-arginine (TAT) signal peptide, were chemically synthesized (Genscript, Piscataway, NJ, USA) and cloned in frame with 6xHis-Tag as *Nco*I/*Xho*I fragments into a shuttle-vector *E. coli-Rhodococcus*, pTipQC2 (containing ampicillin resistance gene for *E. coli* selection and chloramphenicol resistance gene for *Rhodococcus* spp. selection) (Nakashima and Tamura, 2004), obtaining pTipQC2-LMCO2 and pTipQC2-LMCO3. *E. coli* DH5α was transformed by electroporation with recombinant plasmids and selected on LB plus ampicillin (100 μg mL^{-1}) (Sambrook and Russell, 1989). Extracted and purified recombinant plasmids with NucleoSpin Plasmid Kit (Machery and Nagel, Italy) were used to transform *R. erythropolis* AP cells by electroporation (Zampolli et al., 2014). *R. erythropolis* AP cells were selected on LB agar plus chloramphenicol (50 μg mL^{-1}) at 30 °C for 3–4 days.

2.4. Production and purification of recombinant LMCOs

The production of recombinant LMCO2 and LMCO3 was preliminarily assessed by measuring the enzymatic activity of *R. erythropolis* AP cells bearing pTipQC2-LMCO2 and pTipQC2-LMCO3, respectively. *R. erythropolis* AP bearing empty pTipQC2 plasmid was used as a negative control. When the recombinant strain growth reached OD_{600} ~0.6, expression of recombinant enzymes was induced by adding 1 μg mL^{-1} thiostrepton and 250 μM $CuSO_4$ (Santo et al., 2013) and then incubated at 30 °C for 20 h. Induced cells corresponding to 30 OD_{600} was harvested by centrifugation, resuspended in 50 mM potassium phosphate buffer (pH 7, PPB), and incubated with 50 mg mL^{-1} lysozyme at 30 °C for 1 h after vortexing for 10 min. Cells were lysed by sonication (10 cycles of 20 s with 20% amplitude) with a Digital Sonifier™ (BRANSON Ultrasonic Corporation, Italy), and the soluble protein fraction was obtained by centrifugation at 4000 rpm for 10 min at 4 °C. Laccase enzymatic activity of the soluble protein fraction was determined as described in (Zampolli et al., 2021), also by adding 250 μM $CuSO_4$. The specific activity was calculated as U mg^{-1} and reported as the mean of three replicates ± standard deviation (SD). The significant differences were assessed by Student's t-test, showing * p-value < 0.05, or ** p-value < 0.01.

Recombinant LMCO2 and LMCO3 were produced in LB-P medium (5 g L^{-1} yeast extract, 10 g L^{-1} tryptone, 2 g L^{-1} glycerol, and 250 μM $CuSO_4$) added with chloramphenicol (50 mg L^{-1}) and induced as described above for 48 h. Cells were harvested by centrifugation at 4000 rpm at 4 °C, resuspended in lysis buffer (50 mM sodium phosphate buffer (PB) pH 8.0, 300 mM NaCl, and 10 mM imidazole), and lysed twice using a cell disruptor (Constant Systems Ltd) at 30000 psi. The centrifuged crude extracts (12,000 rpm at 4 °C) were purified by metal ion affinity chromatography on a nickel-nitrilotriacetic acid agarose resin (Jena Bioscience, Germany). Samples with the highest protein amount were pooled and buffer-exchanged twice by gel filtration on PD10 columns (GE Healthcare, Little Chalfont, UK) against 10 mm PB, pH 6.0. The determination of protein concentration and SDS-PAGE analysis were carried out as described in (Mangiagalli et al., 2020).

2.5. LMCO2 and LMCO3 biochemical analysis

Enzymatic assays were performed on 2,6-dimethoxyphenol (2,6-DMP) in activity buffer (50 mM tartrate buffer added with $CuSO_4$ 200 μM). The activity was followed for 2 min monitoring the increase in absorbance at 468 nm (ε: 14.8 mM^{-1} cm^{-1}) with a V770 UV/NIR Jasco spectrophotometer (Jasco Corporation, Japan). A mixture containing the activity buffer and 2,6-DMP at the appropriate concentration was used as a blank. One unit of enzyme activity was defined as the amount of enzyme that oxidized 1 μmol of 2,6-DMP per minute.

The optimal temperature of catalysis (T_{opt}) was determined on 2,6-DMP at a final concentration of 4 mM in the temperature range from 15 °C to 80 °C in the activity buffer at pH 7 and 5.5 for LMCO2 and LMCO3, respectively. The optimal pH (pH $_{opt}$) was determined on 2,6-DMP (final concentration 4 mM) in the pH range 4.5–11 in the activity buffer at 65 °C and 80 °C for LMCO2 and LMCO3, respectively.

Reactions were started by adding 0.005 IU of the enzyme to 1 mL of the reaction mix. Long-term thermal stability was monitored by measuring the residual activity after incubating the enzyme (0.5 mg L^{-1}) in PB, pH $_{opt}$, at 35 °C and 65 °C.

Substrate specificity was determined at the optimal catalysis conditions with 2,6-DMP, 2,2'-azino-bis (3-ethylbenzothiazoline-6-sulfonic acid (ABTS, 420 nm, ε: 36 mM^{-1} cm^{-1}), and guaiacol (465 nm, ε: 12 mM^{-1} cm^{-1}) at a final concentration of 4 mM, for 2 min. Activity on ABTS was also tested at pH 4, 5.5, and 7.0 under the previously described conditions.

The kinetic parameters of LMCO2 and LMCO3 were measured on 2,6-DMP and ABTS in the range from 0.05 to 6 mM and calculated with the ORIGINLAB software (OriginLab Corporation, Northampton, MA, USA), using the Michaelis–Menten equation. Kinetics parameters with guaiacol as the substrate were not measured due to the low ΔA min^{-1} values. All the experiments were performed in quadruplicate and shown as mean ± SD.

2.6. LMCO2 and LMCO3 biophysical analysis

Circular dichroism (CD) spectra of LMCOs (10 μM in PB) were recorded in a J815 spectropolarimeter (JASCO Europe, Cremella, Lecco) using a 0.1-cm pathlength cuvette. Thermal unfolding was monitored by recording the CD signal at λ of 215 nm from 25 °C to 90 °C with a temperature slope of 1 °C min^{-1}. The UV/visible absorption spectra (20 μM in PB) were collected with a V770 UV/NIR Jasco spectrophotometer (JASCO Europe, Cremella, Lecco) using a 1-cm quartz cuvette at λ in the range 200-−700 nm. Measurements were carried out with a 1-nm data pitch and 50 nm min^{-1} scanning speed. All spectra were corrected for buffer contribution, averaged from two independent acquisitions. All the experiments are reported as the mean of three replicates ± SD.

The quaternary structure of LMCO2 and LMCO3 (0.5 mg mL^{-1}) was determined by size-exclusion chromatography (SEC) with an NGC Quest 10 Plus Chromatography System (Bio-Rad, California, USA) equipped with a Superdex 10/200 column (Amersham Biosciences, Amersham, UK) with a cutoff of 10–600 kDa. Chromatographic separations were carried out in saline PB (10 mM PB, 150 mM NaCl, pH 6) as the mobile phase, at a flow rate of 0.5 mL min^{-1}, recorded at 280 nm. The molecular weight was determined using a calibration curve made with the following standards: M-βGal (450.93 kDa), alcohol dehydrogenase (yeast, 150 kDa), BSA (66.5 kDa), lipase B of *Candida antarctica* (34.7 kDa), green fluorescence protein (27.5 kDa), and cytochrome C (horse heart, 12.4 kDa).

For each standard protein, the distribution coefficient (K_d) was calculated using the following equation: $K_d = VE\text{-}V_0/VT\text{-}V_0$ where V_E is the elution volume, V_0 is the void volume, which is determined with blue dextran (2000 kDa), and V_T is the total volume, determined with Uracil (0.112 kDa). The calibration curve Log(MW) *vs* K_d was built and the interpolated linear equation was used to calculate LMCO2 and LMCO3 molecular weight from their K_d values. Experiments were performed in triplicate.

2.7. Assessment of LMCO2 and LMCO3 oxidative activity on PE

The oxidative activity of R7 LMCO2 and LMCO3 was evaluated using commercial low-density powder PE (Merck Darmstadt, Germany, Mn = 1700 by GPC, Mw = 4000 by GPC, cod. 427772) as substrate (1% *w/v*). Reactions containing 0.1 mg mL^{-1} of each purified LMCO were carried out in 3 mL glass vessels at 60 °C under shaking (120 rpm) in 50 mM PPB and 50 μM $CuSO_4$ (reaction buffer) in a final volume of 1 mL at pH $_{opt}$ up to 48 h. PE incubated in the reaction mix without enzyme was used as the control. The degradation activity was monitored at 0, 24 h, and 48 h by combining FTIR spectroscopy and GC-MSD analysis. The initial low-density PE powder used for this study was assessed by using ATR-FTIR and GC-MSD analyses after dichloromethane (DCM) extraction. Experiments were performed in triplicate.

2.7.1. Fourier transform infrared (FTIR) spectroscopy

Solid particles in the reaction mixtures were deposited onto the single reflection diamond crystal of the device for attenuated total reflection (ATR) measurements and the FTIR spectra were collected between 5000 and 800 cm^{-1}. Measurements were then repeated by forcing the samples into close contact with the diamond crystal using the clamp arm assembly of the device. After PE incubation with LMCO2 and LMCO3 enzymes, in addition to solid particles, liquid droplets separated from the aqueous phase were observed and their ATR-FTIR spectra collected between 5000 and 800 cm^{-1}. Standard PE powder was analyzed under the same experimental conditions.

The ATR-FTIR spectra were measured by the Quest ATR device (Specac, UK) coupled to a Varian 670-IR spectrometer (Varian Australia Pty Ltd.), equipped with a nitrogen-cooled mercury cadmium telluride detector, under the following conditions: 2 cm^{-1} spectral resolution, scan speed of 25 kHz, 512 scan co-additions, triangular apodization.

2.7.2. GC-MSD analyses

Oxidation products were extracted from the enzymatic assay mixtures with one volume of DCM by shaking the glass vessel manually for 15 min. An aliquot of the extracted organic phase was supplied with N,O-Bis(trimethylsilyl)-trifluoroacetamide (BSTFA) for the derivatization with BSTFA:sample ratio equal to 1:3 at 60 °C for 20 min. BSTFA reacts with the polar groups of different compounds generating silylation groups to obtain higher resolution and stability. The extract (1 μL) was analyzed by a 6890 *N* Network gas chromatograph (GC) system (J&W DB-5 ms Ultra Inert GC Column 60 m × 0.25 mm, 0.25 μm, Agilent Technologies, Santa Clara, CA, USA) with He at 99.99% as a carrier gas, coupled to a 5973 Network Mass Selective Detector (MSD, Agilent Technologies) at 70 eV in the scan ion monitoring mode (40–600 Da). The GC injector temperature was 200 °C. Analyses were carried out in split injection mode (split ratio 10.5:1) with the following temperature program: 3 min at 60 °C, 10 °C min^{-1} to 300 °C, and holding this temperature for 6 min. The resulting chromatograms were analyzed using MSD ChemStation E.02.02.1431 (Agilent Technologies, Santa Clara, CA, USA), and unknown compounds were identified by comparing their mass spectra with the NIST11 database. Products with more than 90% similarity with respect to reference mass spectra were considered. The products obtained by LMCO oxidation and measured in the controls were compared and they were classified by product class. The peak areas of considered products were area normalized and the proportion of different product types was calculated accordingly to "compound peak area/total compounds peak area × 100" (Yao et al., 2022).

2.8. Computational analysis

2.8.1. 3D models of LMCO2 and LMCO3

Prediction runs of LMCO2 and LMCO3 3D structures were executed based on the complete amino acid (aa) sequences via ColabFold (Mirdita et al., 2021), an easy-to-use software based on AlphaFold2 (Jumper et al., 2021). Alphafold2-Multimer (Evans et al., 2021) was used for the prediction of the homotrimeric complex of LMCO3. Default settings were kept for MSA, by using the MMseqs2 clustering module, while template search was disabled and the number of recycles was three. Only the top-ranked model for each protein is presented. To model Cu atoms (neglected by the Alphafold2 routine) into T1, T2, and T3 sites, the predicted 3D structures of LMCO2 and LMCO3 were superimposed to selected 3dMCO or 2dMCO, respectively, with full copper content (PDB: 3KW7 and 3GDC).

2.8.2. Density functional theory calculations

Density Functional Theory (DFT) computations were performed using the pure BP86 and hybrid B3-LYP gradient generalized approximation functional (Becke, 1988; Lee et al., 1988). The def-TZVP basis set (Schafer et al., 1994) was used. The resolution-of-identity (RI) technique was adopted to save CPU time (Eichkorn et al., 1997). The water solvent effect has been accounted using the COSMO (Klamt and Schüürmann, 1993) setting a dielectric constant to 80. Dispersion contributions were treated with the D3 approach (Grimme et al., 2010). All calculations were carried out using the TURBOMOLE suite (Ahlrichs et al., 1989). This computational approach was appropriate to represent the electronic properties of Cu-peptide interactions (Arrigoni et al., 2018; Bertini et al., 2018). Charge distribution was evaluated using Natural bond orbital analysis (NBO). The small models include 7 residues for LMCO2 (Asp257, Tyr415, Trp417, His450, Cys498, His503, and Met508; total charge 0) and 8 for LMCO3 (Trp117, His148, Cys192, Leu198, Glu200, His201, Arg204, and Phe235; total charge +1). To avoid unrealistic conformational rearrangements, the Cα have been constrained to their position in the full models.

3. Results

3.1. R. opacus R7 LMCOs selection and cloning

R. opacus R7 multicopper oxidase genes *LMCO2* and *LMCO3*, located on pPDG3 plasmid, were selected because of their up-regulation upon growth on PE (Zampolli et al., 2021). Comparing the LMCO aa sequence with the laccase-like enzyme sequence of *R. ruber* C208 (Santo et al., 2013), known for its role in PE degradation, LMCO2 shared the highest similarity (53%), whilst LMCO3 23% aa similarity. Multiple alignments with other microbial LMCO sequences with the highest identity, *i.e.*, laccase B from *Trametes* sp. AH28-2 (3KW7 *vs* LMCO2, 26% identity) and LMCO from *Arthrobacter* sp. FB24 (3GDC *vs* LMCO3, 70% identity), highlighted that the copper-binding sites in T1 center and T2/T3 are conserved (Figures S1 A and S1B).

Sequence analysis indicates that LMCO2 belongs to the 3dMCO family, whereas LMCO3 is a member of 2dMCOs (Figure S1C). They share 28% of amino acid identity and similarly to LMCO from *R. ruber* C208 (Santo et al., 2013), both R7 LMCOs contain a signal peptide (TAT motif) for the secretion (Zampolli et al., 2021).

To study their role in PE degradation, *LMCO2* and *LMCO3* genes were cloned into the shuttle-vector *E. coli-Rhodococcus* (Nakashima and Tamura, 2004) and transformed into *R. erythropolis* AP (Zampolli et al., 2014). After growth and induction of gene expression with 1 μg mL^{-1} thiostrepton and 250 μM $CuSO_4$, preliminary enzymatic assays using 2,6-DMP indicated that LMCO2 and LMCO3 were produced intracellularly with a specific activity of 0.04 U g^{-1} and 0.12 U g^{-1}, respectively (Fig. 1, no $CuSO_4$ during the enzymatic assay). Notably, both enzymes required the presence of Cu^{2+} during the induction and the enzymatic assays, showing activity values of 0.75 U g^{-1} and 0.41 U g^{-1} for LMCO2 and LMCO3, respectively (Fig. 1, with $CuSO_4$ added during the enzymatic assay).

3.2. LMCO2 and LMCO3 oxidase activity and different biochemical features

3.2.1. Biochemical characterization of LMCO2 and LMCO3

Recombinant enzymes were produced and purified by affinity chromatography with a final yield of 0.2–0.4 mg of pure protein per liter of culture (Fig. 2A and B). The catalysis reactions were carried out on 2,6-DMP as the substrate in the presence of 200 μM $CuSO_4$. LMCO2 showed the highest activity (T_{opt}) at 65 °C (Fig. 2C) and retained 60% activity in the pH range 6.5–7.5, with an optimal pH of 7.0 (Fig. 2D). This enzyme maintained its secondary structure up to 50 °C, whereas at higher temperatures a loss of CD signal was observed with a T_m of 65 °C (Fig. 3A). On the other hand, LMCO3 was found to be active at acidic pH, with a pH $_{opt}$ of 5.5 and residual activity of around 40% at pH 7.0 (Fig. 2D), and exhibited the highest activity (T_{opt}) at 80 °C (Fig. 2C). The secondary structure of LMCO3 remained unaltered in the temperature range 25–75 °C and was completely lost above 85 °C, with a T_m of 80 °C (Fig. 3A), suggesting that at temperatures >85 °C this enzyme is inactive.

Stability assays were carried out by incubating the purified enzymes at 35 °C and 65 °C for several days before measuring residual activity. At 35 °C, the activity of LMCO2 decreased by 10% after one day and was completely lost within four days (Fig. 3B). At 65 °C, we observed a sharp decrease in LMCO2 activity in the first two days of incubation

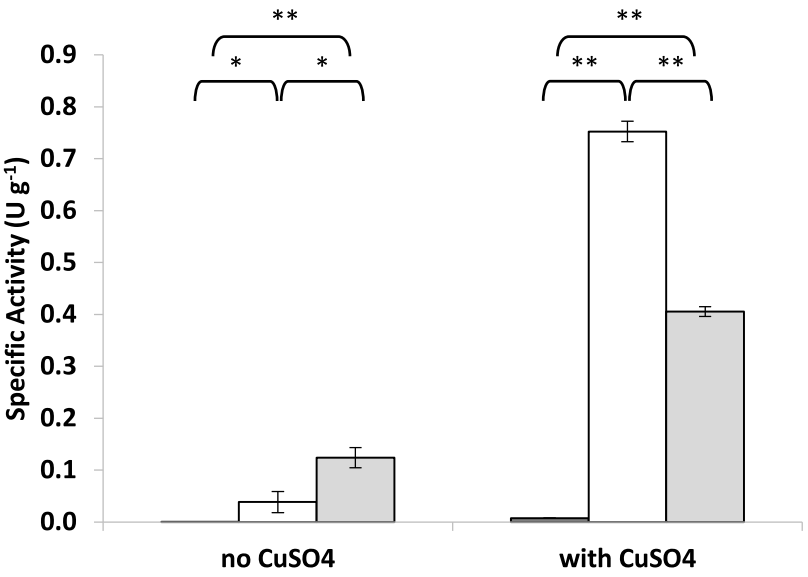

Fig. 1. Oxidase activity of recombinant cell extracts. Oxidase activity of *R. erythropolis* AP recombinant cells carrying *LMCO2* (white) and *LMCO3* (light gray) genes was measured using 30 mM 2,6-DMP in comparison with *R. erythropolis* AP carrying the empty vector, pTipQC2 (dark gray). The laccase activity was measured both in the absence and in the presence of 250 μM $CuSO_4$ during the enzymatic assay. Laccase activity is expressed as U g^{-1} as the mean of three replicates ± standard deviation. Statistical differences were calculated using t-Student's test: * p-value < 0.05, ** p-value < 0.01.

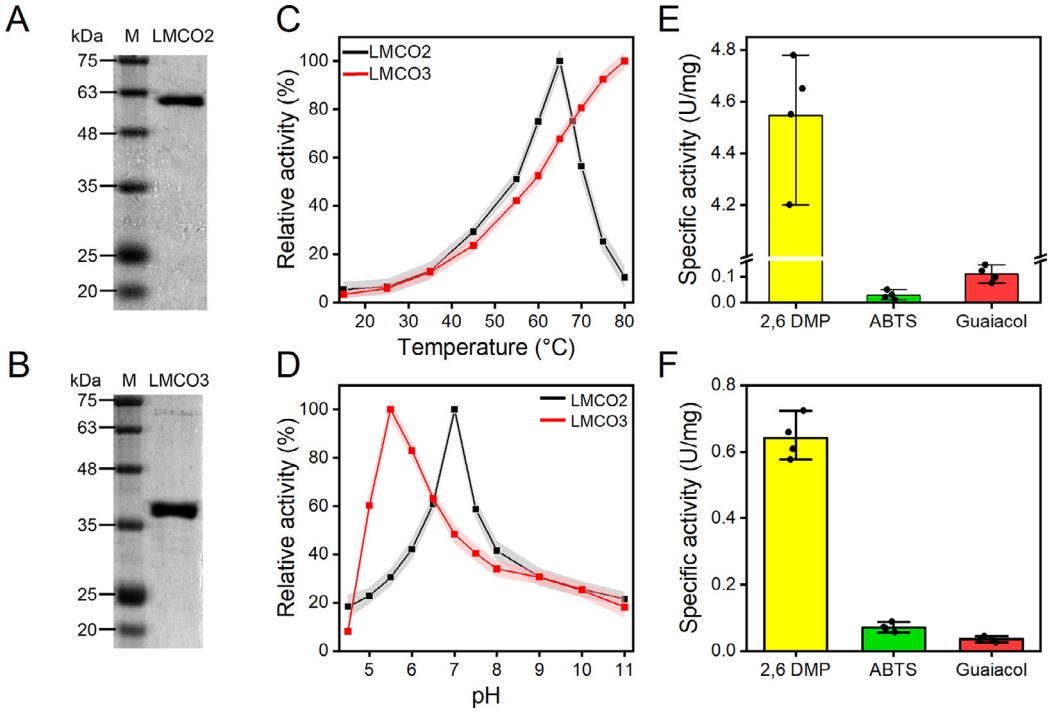

Fig. 2. Biochemical properties of R7 LMCOs. SDS-PAGE analysis of purified LMCO2 (A) and LMCO3 (B); M: molecular weight marker. (C) Effects of temperature on the activity of LMCO2 (black line) and LMCO3 (red line). The temperature profiles were detected using 4 mM 2,6-DMP at pH 7.0 and 5.5, respectively. (D) Effects of pH on the activity of LMCO2 (black line) and LMCO3 (red line). The pH profiles were detected using 4 mM 2,6-DMP at 65 °C and 80 °C, respectively. The substrate specificity of LMCO2 (E) and LMCO3 (F) was determined using 2,6-DMP, ABTS, and guaiacol at the optimal catalysis conditions at a substrate concentration of 4 mM. All experiments were performed in quadruplicate and the shadowed area refers to the standard deviation of the data (n = 4). (For interpretation of the references to color in this figure legend, the reader is referred to the web version of this article.)

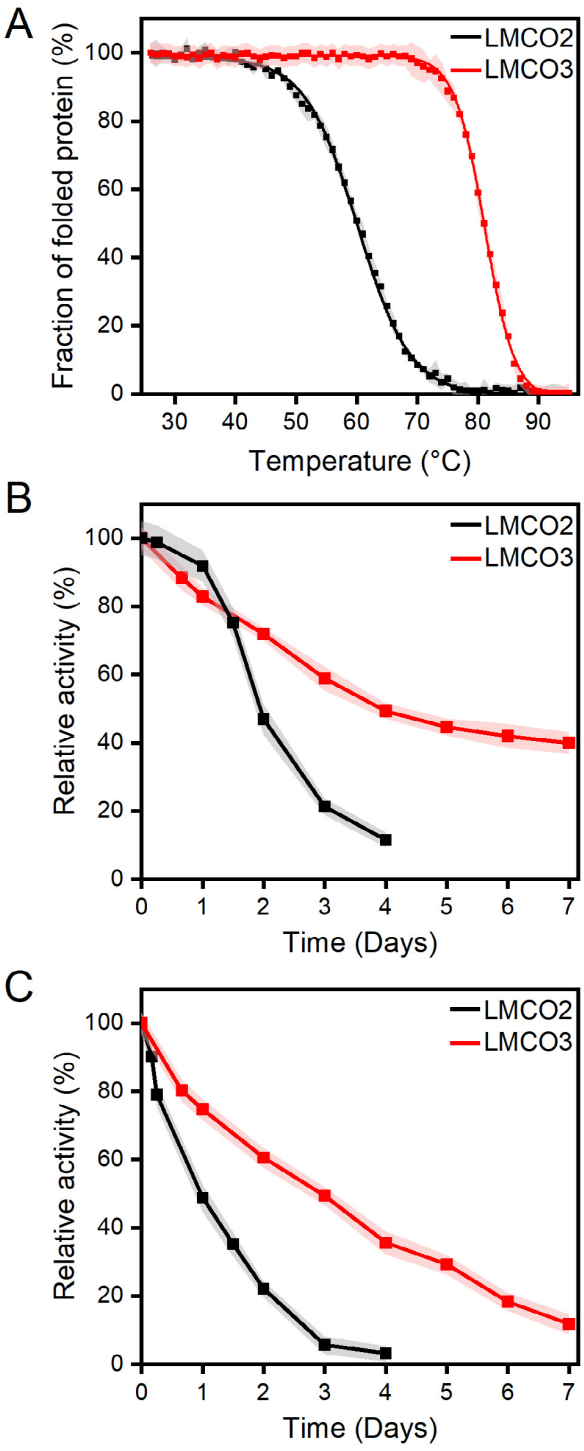

Fig. 3. Thermal stability of R7 LMCOs. Thermal stability of LMCO2 (black line) and LMCO3 (red line) (A). Ellipticity values were recorded at 205 nm during heating from 25 to 95 °C. The initial CD signal was taken as 100% for normalization. Long-term thermal stability (B–C) of LMCO2 (black line) and LMCO3 (red line). Thermal stability over time was measured by incubating the enzyme at 35 °C (B) and 65 °C (C) and shown as residual activity obtained with 2,6-DMP as a substrate. All the experiments were performed in quadruplicate and the shadowed area refers to the standard deviation of the data (n = 4).. (For interpretation of the references to color in this figure legend, the reader is referred to the web version of this article.)

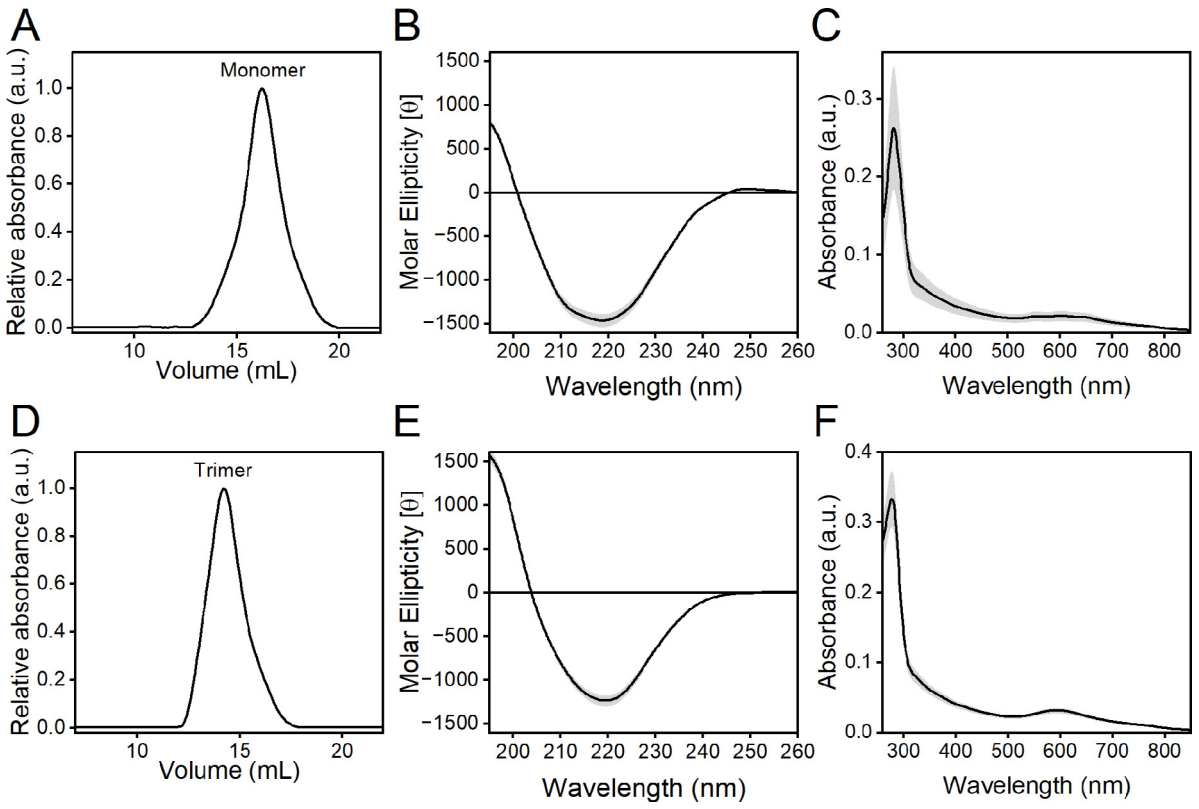

Fig. 4. Structural features of LMCO2 and LMCO3. Oligomerization state of LMCO2 (A) and LMCO3 (D) as determined by SEC analysis. One out of three independent measurements is shown. Far-UV CD spectra of LMCO2 (B) and LMCO3 (E) collected in PB at 25 °C. UV/Vis absorption spectra of LMCO2 (C) and LMCO3 (F) collected in PB at 25 °C. All the experiments were performed in triplicate and the shadowed area refers to the standard deviation of the data (n = 3).

and its complete inactivation within the third day (Fig. 3C). By contrast, LMCO3 retained 40% and 15% of residual activity after 7 days of incubation at 35 °C and 65 °C, respectively (Fig. 3B and C). Overall, both enzymes are more thermostable than the previously reported LMCOs from *R. ruber* C208 and *Psychrobacter* sp. NJ228 for PE degradation (Santo et al., 2013; Zhang et al., 2022a).

LMCO2 and LMCO3 oxidize both phenolic (*i.e.,* 2,6-DMP and guaiacol) and non-phenolic (*i.e.,* ABTS) compounds (Fig. 2E and F). The highest activity for both enzymes was towards 2,6-DMP, with the specific activity of LMCO2 10-times higher than that of LMCO3. As reported in other LMCOs (Reiss et al., 2011), the activity of LMCO2 towards ABTS is higher at pH 4.0 than at pH 5.5 and 7.0 (Figure S2). The analysis of kinetics parameters (Table S2) indicates that LMCO2 has a lower affinity towards 2,6-DMP (K_M 1.14± 0.02 mM) and ABTS (K_M 1.63± 0.12 mM) than LMCO3 (K_M 0.36± 0.01 mM and K_M 0.28± 0.02 mM for 2,6-DMP and ABTS, respectively).

In conclusion, our results indicate that LMCO2 and LMCO3 are multicopper oxidases showing the highest activity on 2,6-DMP, and different biochemical features in terms of optimal pH, temperature, substrate specificity, and thermal stability.

3.2.2. LMCO2 and LMCO3 structural characteristics

The structural features of the two enzymes were studied by SEC, CD, and UV/Vis absorption spectroscopies. SEC analysis on purified enzymes indicates that LMCO2 is a monomer with a molecular mass of 53 kDa, while LMCO3 is a trimer (128 kDa) (Fig. 4A and D).

The Far-UV CD spectra of both proteins are characterized by a minimum peak at ~218 nm, typical of proteins rich in β-structure (Fig. 4B and E). The UV/Vis absorption spectra show a peak at ~610 nm, typical of paramagnetic Type I (T1) copper sites (Jones and Solomon, 2015) of blue laccases (Fig. 4C and F). Overall, these structural features are typical of 2dMCO and 3dMCO (Gräff et al., 2020) and are consistent with the 3D structural models described in paragraph 3.4.

3.3. LMCO2 and LMCO3 oxidization activity on PE powder

On the basis of the biochemical characterization, LMCO2, and LMCO3 enzymes were individually evaluated for their oxidative ability towards commercial low-density PE powder in the presence of 50 μM $CuSO_4$ at 60 °C up to 48 h in

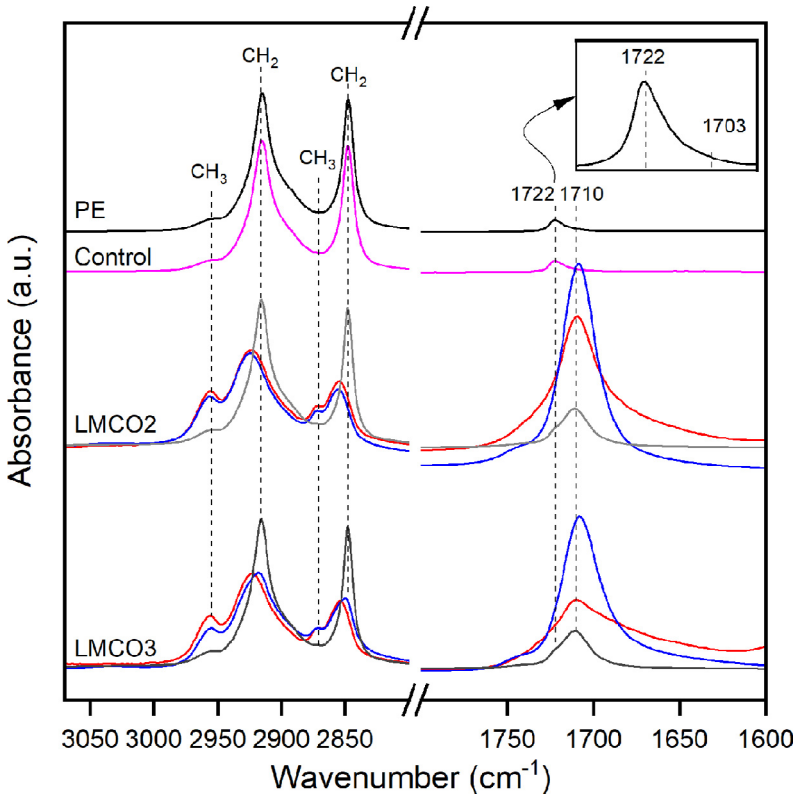

Fig. 5. FTIR analysis of enzymatic degradation of PE. The FTIR spectra of PE powder as is and incubated for 24 h at 60 °C, without enzymes, are shown in black and magenta lines respectively. The FTIR spectra of liquid droplets (blue line) and PE particles (red line) were collected after incubation for 24 h at 60 °C in the presence of LMCO2 and LMCO3. The FTIR spectra of PE particles pressed on the ATR diamond crystals are shown as gray lines. One of three independent measurements was shown. (For interpretation of the references to color in this figure legend, the reader is referred to the web version of this article.)

comparison to the same conditions without the enzymes. The temperature of 60 °C was chosen due to the T_{opt} and the long-term thermal stability of LMCO2 and LMCO3; in addition, at this temperature, the PE polymer is more accessible to enzymes (Fontanella et al., 2010; Abrusci et al., 2011). FTIR spectroscopy was performed to obtain data on PE oxidative degradation in terms of the potential chemical bond breakage, the changes in functional groups, and the transformation of the molecular structures (Zhang et al., 2022b); GC-MSD analyses were performed to detect the released products. The commercial low-density PE powder was preliminarily analyzed by using both techniques. The ATR-FTIR spectrum shows two main peaks at ∼2916 and ∼2848 cm^{-1}, due to antisymmetric and symmetric CH_2 stretching, respectively, and a C=O absorption at ∼1722 cm^{-1}, with a shoulder around 1703 cm^{-1}, assigned mainly to carboxylic acids and ketones (black line in Fig. 5) (Sandt et al., 2021). After DCM extraction, the GC-MSD analyses evidenced mostly alkanes and ketones with carbon chain lengths mainly ranging between C12 and C25, and carboxylic acids (only with carbon chain lengths of C16 and C18) (Figure S3). The initial PE analyses suggested a partial oxidation of the polymer.

3.3.1. FTIR spectroscopy for the characterization of PE oxidized products

The effect of LMCO activity on PE was assessed by ATR-FTIR spectroscopy (Fig. 5). The ATR-FTIR spectrum of PE measured after 24 h in the absence of the enzymes (magenta line in Fig. 5) is superimposable to that of commercial PE, indicating that the incubation in reaction buffer at 60 °C does not affect the polymer structure. After 24 h of incubation in the presence of LMCO2 and LMCO3, we observed a heterogeneous suspension of PE particles and liquid droplets, visible on the wall of the glass vials (arrows in Figure S4). The ATR-FTIR spectra of the liquid droplets and PE particles (Fig. 5 and Figure S5) display spectral features typical of carboxylic acids, as indicated by the C=O band at ∼1710 cm^{-1}, and a well-resolved hydrocarbon chain absorption between 3050 and 2800 cm^{-1} (Casal and Mantsch, 1984). Furthermore, we noticed that when the PE particles are pressed on the ATR diamond crystals, their FTIR spectrum appears similar to that of commercial PE, with the relative intensity of C=O peak at ∼1710 cm^{-1} with respect to the 3050–2800 cm^{-1} CHx band, strongly reduced in comparison to that observed in the droplet spectrum (Figure S5). Comparable results were obtained for the two enzymes, LMCO2 and LMCO3, after 24 h and 48 h (data not shown) of incubation. Overall, these results indicate that the enzymatic PE oxidation leads mainly to the formation of carboxylic acids, which generate droplets in suspension

Table 1
Partial products of PE oxidation by LMCO2 and LMCO3 obtained through GC-MSD analyses after 24 h. Numbers in brackets from 1 to 12 indicate the major identified products in the chromatograms of Fig. 6.

Compound[a]	Retention Time (t_R) (min)	Formula	CAS number	LMCO2	LMCO3	No enzyme[b]
Benzoic acid	13.5	C7H6O2	65-85-0	+[c]	+	–
Octanoic acid (1)	13.8	C8H16O2	124-07-2	+	+	+
2-Undecanone	14.2	C11H22O	112-12-9	+	+	–
Nonanoic acid (2)	15	C9H18O2	112-05-0	+	+	–
Decanoic acid, ethyl ester	15.5	C12H24O2	110-38-3	+	+	–
2-Dodecanone	15.6	C12H24O	6175-49-1	+	+	–
Decanoic acid (3)	16.3	C10H20O2	334-48-5	+	+	–
Hexanedioic acid (8)	16.9	C6H10O4	124-04-9	+	+	–
Dodecanoic acid, methyl ester	17.2	C12H24O2	143-07-7.	+	+	–
Dodecanoic acid, ethyl ester	18.1	C14H28O2	106-33-2	+	+	–
1-Dodecanol	17.7	C12H26O	112-53-8	+	+	–
2-Tetradecanone (9)	18.2	C14H28O	2345-27-9	+	+	+
Dodecanoic acid	18.7	C12H24O2	143-07-7	+	+	–
Cyclododecane	19.3	C12H24	294-62-2	+	–	–
Heptadecane	19.4	C17H36	629-78-7	+	+	+
2-Hexadecanone (10)	20.5	C16H32O	18787-63-8	+	+	+
Tetradecanoic acid	20.9	C14H28O2	544-63-8	+	+	–
n-Pentadecanoic acid	21.9	C15H30O2	1002-84-2	+	+	–
Octanoic acid 2-octyl ester	22.3	C16H32O2	55193-33-4	+	+	–
Methyl *n*-hexadecyl ketone (11)	22.6	C18H36O	7373-13-9	+	+	+
Hexadecanoic acid (4)	22.9	C16H32O2	57-10-3	+	+	+
Heptadecanoic acid	23.8	C17H34O2	506-12-7	+	+	–
2-Nonadecanone (12)	24.5	C19H38O	629-66-3	+	+	+
Octadecanoic acid (5)	24.7	C18H36O2	57-11-4	+	+	+
Eicosane	25.3	C20H42	112-95-8	+	–	–
Tetracosane	26.1	C24H50	646-31-1	+	–	–
2-Docosanone (6)	26.2	C22H44O	77327-11-8	+	+	+
Pentacosane (7)	26.9	C25H52	629-99-2	+	+	–
Heptacosane	28.6	C27H56	593-49-7	+	–	–
Octacosane	30.7	C28H58	630-02-4	+	+	–
Triacontane	32.1	C30H62	638-68-6	+	–	–

[a]Compound, considered degradation products had >90% similarity by comparing their mass spectra with the NIST11.
[b]No enzyme, reaction assay established in PPB and PE without the enzymes.
[c]+, the symbol "+" indicates the products, while "–" indicates the absence.

that adhere to the vial wall (Figure S4) and to the polymer where it can be removed by the mechanical action of the ATR press.

3.3.2. Oxidized products deriving from PE biodegradation

In order to comprehend the mechanism behind the PE enzymatic attack and to characterize the degradation products obtained by LMCO2 and LMCO3, DCM solvent extraction and GC-MSD analyses were performed up to 48 h in comparison to the condition without the enzymes. Fig. 6, and Table 1 show the results at 24 h evidencing different alkyl and oxygenated products with carbon chain lengths mainly ranging between C8 and C30; in particular, alkanes showed a carbon chain length range of C12-C30, 2-ketones of C11-C19, alcohols only C10, and carboxylic acids of C8-C18. Interestingly, the main product type was carboxylic acid (99% normalized peak area) (Figure S6). The two laccases showed the same kind of accumulated products at 24 h with only a few differences in the presence of a higher number of alkane types in LMCO2 reaction with respect to LMCO3 (Figure S6 and Table 1).

The chromatographic profile at 48 h of PE oxidation by LMCOs was quite similar to that recorded at 24 h, with a few exceptions; notably, for LMCO3 we observed the presence of alkanes with a number of carbon chain lengths major than C20 (Figure S7).

Overall, the GC-MS LMCO profiles differ with respect to the condition without enzymes that instead appears similar to the commercial PE with only slight differences with respect to the initial polymer.

In addition, a small aromatic compound (benzoic acid) was evidenced (Table 1) and confirmed by ATR-FTIR analyses. This plastic antioxidant is normally present in polymers as an additive and the presence after 24 h of enzyme reaction could be associated with its release from the PE structure (Arendt et al., 2019; Yao et al., 2022; Sanluis-Verdes et al., 2022).

3.4. A computational model of LMCOs from R. opacus R7

The most challenging aspect of PE oxidation by LMCO2 and LMCO3 is the understanding of the most likely catalytic mechanism of substrate oxidation. To analyze LMCO structural features, a structural model of these enzymes was

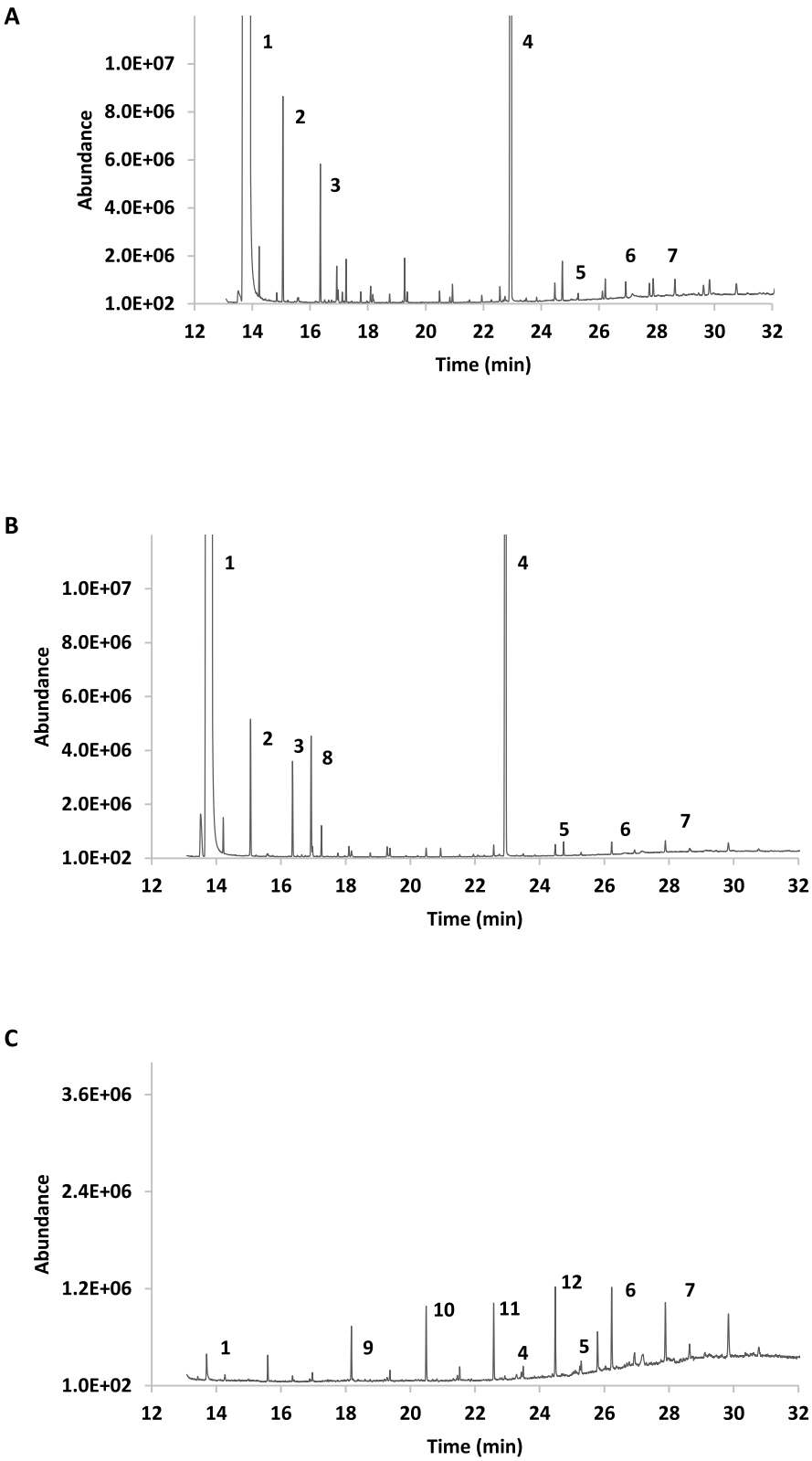

Fig. 6. Product profile of R7 LMCO oxidation of PE by GC-MSD analysis. GC-MSD chromatogram profiles of derivatized product extracts deriving from PE oxidation at 24 h by LMCO2 (A) and LMCO3 (B) with respect to the condition in the absence of the enzymes (C). The numbered peaks correspond to 1, octanoic acid; 2, nonanoic acid; 3, decanoic acid; 4, hexadecanoic acid; 5, octadecanoic acid; 6, 2-docosanone; 7, pentacosane; 8, hexanedioic acid; 9, 2-tetradecanone; 10, 2-hexadecanone; 11, methyl *n*-hexadecyl ketone; 12, 2-nonadecanone.

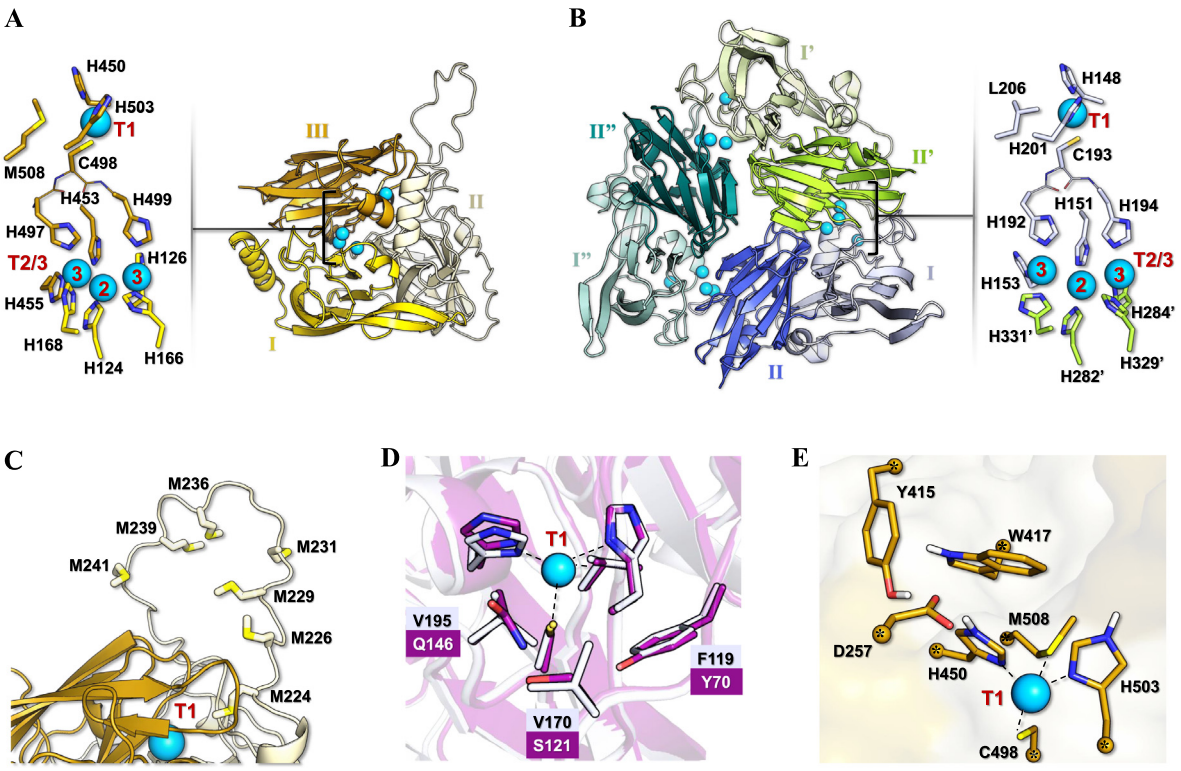

Fig. 7. (A) 3D model predicted for LMCO2, with details on T1, T2, and T3 sites. The three domains are indicated as I, II, and III. (B) 3D model predicted for the trimeric LMCO3, with details on T1, T2, and T3 sites. The two domains for each monomer are also indicated as I/II, I'/II', and I"/II". (C) Structural details on the methionine-rich loop of LMCO2, as predicted by Alphafold2. (D) Superimposition of T1 site for LMCO3 (light blue) and 3GDC (in purple). (E) DFT optimized structure of LMCO2 small model. The atoms that have been kept fixed during geometry optimizations are indicated by an asterisk. (For interpretation of the references to color in this figure legend, the reader is referred to the web version of this article.)

generated. Since the oxidation of the substrate in laccase enzymes is always mono-electronic, the aliphatic carbon radical species may be produced, thus DFT calculations were performed to shed light on the chemical feasibility of this process.

LMCO2 and LMCO3 3D models predicted with Alphafold2 are typical respectively of 3dMCO and 2dMCO (Fig. 7A and B), as also supported by the superimposition of both models with references (3KW7 for LMCO2 and 3GDC for LMCO3). Both predicted models are characterized by high confidence, as evidenced by the average lDDT value (>= 85, for further details see Figure 1 in Supplementary S8). The proteins also showed the copper-binding sites in the T1 center (His450, Cys498, and His503 for LMCO2; and His148, Cys193, and His201 for LMCO3) and in the T2/T3 centers (His124, His126, His166, His168, His453, His455, His497 and His499 for LMCO2; His151, His153, His192, His194, His282, His284, His329, and His331 for LMCO3) (Fig. 7A and B, Figure S1). In LMCO2, the ligands setting is compatible with the presence of four metal-binding sites, as in all 3dMCOs (Arregui et al., 2019). The first site, characterized by a distorted tetrahedral geometry typical of the T1 site, is composed of two His, one Cys, and one Met, all belonging to domain III (Rovaletti et al., 2023). The others have instead the typical features of two T3 and one T2 sites (Solomon et al., 2014), for a total of eight coordinating His, four parts of domain III, and the other four of domain I.

Met-loops of different compositions and lengths have been observed in diverse prokaryotic laccases, including in R7 LMCO2 (residues 224–241) in proximity to the T1 site (Fig. 7C) (Serrano-Posada et al., 2011; Granja-Travez et al., 2018; Borges et al., 2020). The presence and the properties of this Met-rich motif have been recently linked to catalytic activity modulation, substrate interaction, and selectivity, affecting the kinetics of the rate-limiting step *i.e.*, electron transfer from substrate to T1 Cu by a Marcus outer-sphere mechanism (Solomon et al., 2014; Borges et al., 2020). Interestingly, these properties indicate a strong propensity to bind hydrophobic carbon-based surfaces (Cui et al., 2021).

Besides being a 2dLMCO, LMCO3 presents two remarkable differences with respect to LMCO2: (i) the T1 site features a Leu (Leu206) instead of a Met in the axial position, having a three-coordinated trigonal planar structure, and (ii) one monomer is not enough to provide the full T2/T3 coordination environment which can be formed only if trimerization is invoked; thus, domain I of one monomer and domain II of the adjacent one can participate with four His residues each (Janusz et al., 2020). Structural comparison between LMCO3 and other 2dMCOs revealed some differences in T1 surroundings.

Moreover, one of the structural determinants of T1 laccases redox potential (RP) is the nature of the axial ligand: the higher the T1 RP is, the wider the range of processed substrates (Macellaro et al., 2014; Barber-Zucker et al., 2022). In

general, 2dLMCOs are low-potential systems, with a T1 RP in the range of 0.35–0.45 V (Trubitzina et al., 2021; Rovaletti et al., 2023). Although the T1 oxidizing power can be modulated by several factors, the presence of a non-coordinating Leu has been associated with an increase in RP (Xu et al., 1996; Li et al., 2004; Cambria et al., 2012), as in the case of fungal laccase in *Melanocarpus albomyces* (3FU7, Kallio et al., 2009).

In fact, a tri-coordinated Cu^{2+} center should be more prone to reduction with respect to a four-coordinated one, in light of its lower electron-richness. A structural comparison of T1 surroundings between LMCO3 and 3GDC (Fig. 7D) revealed that Y70, Q146, and S121 in 3GCD are replaced by F119, V170, and V195 in LMCO3, suggesting a higher hydrophobicity of the latter. Interestingly, the T1 site is also characterized by a less negative net charge ($q = -2$, calculated as the sum of charged residues found in a sphere centered on Cu of a 12 Åradius) if compared to other characterized 2dLMCOs (Supplementary S8) such as (3GDC, $q = -3$), 4M3H ($q = -3$), 3TAS ($q = -4$), 2ZWN ($q = -4$), 5LHL ($q = -4$) and 3G5 W ($q = -6$). All these considerations raise the possibility that LMCO3 should have a slightly higher RP with respect to others 2dLMCOs, since the lower polarity of T1 surroundings should stabilize the Cu(I) state, thus favoring Cu reduction/substrate oxidation (Li et al., 2004; Cambria et al., 2012).

The simulation of LMCO2 and LMCO3 binding to the PE surface is challenging for the lack of experimental data on the nature of their interaction but it is known in the literature that laccases can bind hydrophobic substrates and process several non-phenolic compounds (Xu et al., 2020). For this reason, the following DFT calculations were focused on the evaluation of the propensity to oxidize aliphatic C–H bonds of the PE based on the experimental evidences mostly suggesting the formation of new carbonyl groups (Figure S6). In order to evaluate such hypothesis, we carried out DFT computations considering a small portion of the laccase binding pocket bound to a model substrate (Supplementary S8). The whole model includes (i) T1 Cu coordination sphere plus an Asp/Glu residue involved in the electron/proton transfer from the substrate to the T1 Cu site which is considered the rate-determining step in laccase catalytic cycle (Mehra and Keep, 2019); (ii) residues involved in the stabilization of Asp/Glu-His interaction (Tyr415 and Trp417 for LMCO2; Arg205, Trp117, and Phe235 for LMCO3) (Chiadò et al., 2021); (iii) a small portion (C7 moiety) of the entire polymer which models the PE portion bound at laccase pocket. Here, we are investigating the first of the two mono-electron oxidations which lead to the oxidation of a C–H bond to the corresponding alcohol (Rovaletti et al., 2023). The extended PE structure, on the other hand, will clearly influence the binding to the enzyme pocket but much less its oxidation.

The energy difference (ΔE_r) between the T1 Cu/PE aliphatic portion and its electron/proton transfer form can be useful to assess the propensity of the enzyme to oxidize the substrate. The ΔE_r values obtained for the PE model (Supplementary S8) are generally less than 31.3 kcal mol^{-1}, being the lowest value found for secondary radical products, obtained equal to 22.7 kcal mol^{-1} for LMCO3.

For sake of comparison, the ΔE_r value was computed for 2,6-DMP with both models (Supplementary S8), resulting in the lowest ΔE_r value for LMCO2 of 7.3 kcal mol^{-1}, which is 15.4 kcal mol^{-1} lower compared to the lowest value for the PE model. This is in line with the much higher stability of phenolic radicals compared to aliphatic ones.

4. Discussion

The issue of plastic production and consequent waste is ever-increasing, thus, multiple approaches address this challenge (Yeung et al., 2021; Andler et al., 2022). Among them, both bacteria biodegradation and enzymatic oxidation can be applied for efficient and sustainable processes (Restrepo-Flórez et al., 2014). Bacteria of *Rhodococcus* genus are of great relevance for their extraordinary metabolic potential, also towards plastic polymers (Zampolli et al., 2022, 2018). Considering the few members of *Rhodococcus* genus able to biodegrade PE (Santo et al., 2013; Eyheraguibel et al., 2017; Zampolli et al., 2021), *R. opacus* R7 was studied for its ability to degrade untreated PE in a short range of time by RNA-seq analysis revealing the up-regulation of genes encoding LMCOs (Zampolli et al., 2021).

To establish the role of LMCOs in the PE biodegradation pathway in R7 strain, two novel multicopper oxidases, LMCO2 and LMCO3, were characterized and tested for their oxidative ability towards PE. Based on the number of cupredoxin-like domains (Janusz et al., 2020), *LMCO2* is classified as 3dMCO and *LMCO3* as 2dMCO. Both R7 LMCOs contain a signal peptide (TAT motif) for the secretion, as reported in the LMCO from *R. ruber* C208 (Santo et al., 2013). Our results suggested that Cu^{2+} plays a key role in the activity of R7 LMCOs, as already reported for LMCO from *R. ruber* C208, whose activity towards PE increases by 75% in the presence of Cu^{2+} (Santo et al., 2013).

Moreover, LMCO2 and LMCO3 exhibit different functional features in terms of substrate specificity, pH_{opt}, temperature dependence, and thermal stability, suggesting that the production of different LMCOs would allow *R. opacus* R7 to oxidize a broad range of substrates, including phenolic and non-phenolic compounds, in different pH environments. These results together with the presence of a signal peptide suggests that LMCO2 and LMCO3 are secreted in the extracellular environment, where they could play a role in the oxidation and/or degradation of the untreated PE powder. To test this hypothesis, the ability of R7 LMCOs to oxidize low-density untreated PE was investigated. Low-density PE is generally more accessible to enzymatic treatment because of its amorphous structure with branched short chains of 10–30 C for every 1000 C atoms (Montazer et al., 2019; Yao et al., 2022).

FTIR spectroscopy indicated that PE was oxidized to carboxylic acids in the presence of R7 LMCOs. These oxidation products can be found as droplets in suspension or adhere to the polymer. Our data are in line with those obtained with other microbial LMCOs (Yao et al., 2022; Zhang et al., 2022a). Interestingly, in the presence of R7 LMCOs, the oxidation products were observed after one day of incubation, a shorter time compared with other microbial LMCOs

such as C208 laccase (Santo et al., 2013), PsLAC (Zhang et al., 2022a), and *T. versicolor* LMS (Fujisawa et al., 2001). In addition, similar to PsLAC (Zhang et al., 2022a), R7 LMCOs did not require mediators such as 1-hydroxybenzotriazole (HBT), or 2,2,6,6-tetramethylpiperidin-1-yloxy (TEMPO) to oxidize PE (data not shown).

In agreement with FTIR results, GC-MSD analyses showed that the oxidation products of PE consisted mainly of carboxylic acids and small amounts of alkyls, ketones, and alcohols. The oxidation product pattern is similar for both the enzymes, with some differences in the composition of alkanes: short-chain alkanes were obtained after 24 h of incubation with LMCO2, while long-chain alkanes were observed after 48 h of incubation with LMCO3. The presence of alkanes could be due to the degradative processes of PE or its oxidative products. A similar oxidation pattern has been also reported when the PE was oxidized by the laccase from *Botrytis aclada* (BaLac) and *Bacillus subtilis* (BsLac) with three different mediators (ABTS, HBT, and TEMPO) (Yao et al., 2022). Moreover, GC-MSD analysis highlighted the release of benzoic acid, a common additive used during the PE polymerization process as observed by Sanluis-Verdes and coworkers (Sanluis-Verdes et al., 2022).

To shed light on the chemical feasibility of the PE oxidation process suggested by experimental data, we predicted the 3D structure of R7 LMCOs and performed DFT calculations. According to our structural analysis, LMOC3 should have a slightly higher RP compared to other 2dLMCOs, suggesting a higher catalytic activity and a wide substrate specificity. On the other hand, LMCO2 could bind PE through a Met-rich hydrophobic loop near to the T1 center, absent in LMCO3. Subsequently, with the idea of verifying whether the C–H bonds can undergo electron/proton transfer by T1 Cu, the DFT energy difference was calculated between reactants and products following the first mono-electronic oxidation step which is known to be the rate determining step of the laccase catalytic process. Although these calculations cannot be considered exhaustive of the description of this process, they suggest that the formation of a radical aliphatic species cannot be excluded. This process would be characterized by a higher energy barrier compared to those of the typical phenolic substrates, as suggested by kinetic experiment and DFT computations using 2,6-DMP as a substrate. Once the radical is formed, it could undergo a further second oxidation step followed by a water nucleophilic attack yielding the corresponding secondary/tertiary alcohol (Scheme 4 in Supplementary S8). Speculating on the subsequent oxidative steps and having in mind the laccase catalytic mechanism, the alcohol group could undergo further oxidation with the formation of an alkoxide radical that evolves to carbonyl, as proposed for anthracene and benzo[a]pyrene laccase degradation to the correspondent quinones (Zeng et al., 2011; Guan et al., 2018).

In conclusion, our results provide key new insights into PE oxidative degradation by laccase-like enzymes from a strain belonging to *Rhodococcus* genus. This outcome is even more valuable because of the possibility to exploit both the catalytic activity of *R. opacus* R7 laccases to oxidize PE generating a complex mix of aliphatic and oxygenated products and its impressive metabolic potential that allow PE mineralization.

Funding

This paper was founded by Mur Project ATE-0460 Project 2021.

CRediT authorship contribution statement

Jessica Zampolli: Conceptualization, Methodology, Investigation, Formal analysis, Visualization, Writing – original draft, Writing – review & editing. **Marco Mangiagalli:** Validation, Investigation, Visualization, Writing – original draft. **Daniele Vezzini:** Investigation, Validation. **Marina Lasagni:** Methodology, Curation, Resources. **Diletta Ami:** Methodology, Validation, Investigation. **Antonino Natalello:** Software, Formal analysis, Visualization. **Federica Arrigoni:** Methodology, Software, Formal analysis, Visualization. **Luca Bertini:** Software, Formal analysis, Resources, Data curation. **Marina Lotti:** Conceptualization, Resources, Supervision. **Patrizia Di Gennaro:** Conceptualization, Resources, Funding acquisition, Writing – review & editing.

Declaration of competing interest

The authors declare that they have no known competing financial interests or personal relationships that could have appeared to influence the work reported in this paper.

Data availability

All the research data are available in the manuscript.

Acknowledgments

We thank Arianna Lomasto for her contribution in protein purifications and biochemical experiments and the project "Dipartimenti di Eccellenza 2017" of University of Milano-Bicocca, Department of Biotechnology and Biosciences, Milano, Italy.

Appendix A. Supplementary data

Supplementary material related to this article can be found online at https://doi.org/10.1016/j.eti.2023.103273.

References

Abrusci, C., Pablos, J.L., Corrales, T., López-Marín, J., Marín, I., Catalina, F., 2011. Biodegradation of photo-degraded mulching films based on polyethylenes and stearates of calcium and iron as pro-oxidant additives. Int. Biodeterioration Biodegrad. 65 (3), 451–459. http://dx.doi.org/10.1016/j.ibiod.2010.10.012.

Ahlrichs, R., Bär, M., Häser, M., Horn, H., Kölmel, C., 1989. Electronic structure calculations on workstation computers: The program system turbomole. Chem. Phys. Lett. 162 (3), 165–169. http://dx.doi.org/10.1016/0009-2614(89)85118-8.

Altschul, S.F., Gish, W., Miller, W., Myers, E.W., Lipman, D.J., 1990. Basic local alignment search tool. J. Mol. Biol. 215 (3), 403–410. http://dx.doi.org/10.1016/S0022-2836(05)80360-2.

Amobonye, A., Bhagwat, P., Singh, S., Pillai, S., 2021. Plastic biodegradation: Frontline microbes and their enzymes. Sci. Total Environ. 759, 143536. http://dx.doi.org/10.1016/j.scitotenv.2020.143536.

Andler, R., Tiso, T., Andree"zen, C., Zampolli, J., D'Afonseca, V., Guajardo, C., Díaz-Barrera, A., 2022. Current progress on the biodegradation of synthetic plastics: from fundamentals to biotechnological applications. Rev. Environ. Sci. Biotechnol. 21, 829–850. http://dx.doi.org/10.1007/s11157-022-09631-2.

Arendt, W.D., McBride, E., Roth, S.D., Hatcher, E., 2019. Polyester plasticizers with benzoic acid end-caps. EP3090027B1.

Arregui, L., Ayala, M., Gómez-Gil, X., Gutiérrez-Soto, G., Hernández-Luna, C.E., de los Santos, M.H., Levin, L., Rojo-Domínguez, A., Romero-Martínez, D., Saparrat, M.C.N., Trujillo-Roldán, M.A., Valdez-Cruz, N.A., 2019. Laccases: structure, function, and potential application in water bioremediation. Microb. Cell Fact. 18, 200. http://dx.doi.org/10.1186/s12934-019-1248-0.

Arrigoni, F., Prosdocimi, T., Mollica, L., De Gioia, L., Zampella, G., Bertini, L., 2018. Copper reduction and dioxygen activation in Cu–amyloid beta peptide complexes: Insight from molecular modelling. Metallomics 10, 1618–1630. http://dx.doi.org/10.1039/C8MT00216A.

Barber-Zucker, S., Mateljak, I., Goldsmith, M., Kupervaser, M., Alcalde, M., Fleishman, S.J., 2022. Designed high-redox potential laccases exhibit high functional diversity. ACS Catal. 12 (21), 13164–13173. http://dx.doi.org/10.1021/acscatal.2c03006.

Becke, A.D., 1988. Density-functional exchange-energy approximation with correct asymptotic behavior. Phys. Rev. A 38 (6), 3098–3100.

Bertini, L., Breglia, R., Lambrughi, M., Fantucci, P., De Gioia, L., Borsari, M., Sola, M., Bortolotti, C.A., Bruschi, M., 2018. Catalytic mechanism of fungal lytic polysaccharide monooxygenases investigated by first-principles calculations. Inorg. Chem. 57 (1), 86–97. http://dx.doi.org/10.1021/acs.inorgchem.7b02005.

Borges, P.T., Brissos, V., Hernandez, G., Masgrau, L., Lucas, M.F., Monza, E., Frazão, C., Cordeiro, T.N., Martins, L.O., 2020. Methionine-rich loop of multicopper oxidase mcoa follows open-to-close transitions with a role in enzyme catalysis. ACS Catal. 10 (13), 7162–7176. http://dx.doi.org/10.1021/acscatal.0c01623.

Cambria, M.T., Gullotto, D., Garavaglia, S., Cambria, A., 2012. In silico study of structural determinants modulating the redox potential of *Rigidoporus lignosus* and other fungal laccases. J. Biomol. Struct. Dyn. 30 (1), 89–101. http://dx.doi.org/10.1080/07391102.2012.674275.

Casal, H.L., Mantsch, H.H., 1984. Polymorphic phase behaviour of phospholipid membranes studied by infrared spectroscopy. Biochim. Biophy. Acta Biomembr. 779 (4), 381–401. http://dx.doi.org/10.1016/0304-4157(84)90017-0.

Chiadò, A., Bosco, F., Bardelli, M., Simonelli, L., Pedotti, M., Marmo, L., Varani, L., 2021. Rational engineering of the lcc β *T. versicolor* laccase for the mediator-less oxidation of large polycyclic aromatic hydrocarbons. Comput. Struct. Biotechnol. J. 19, 2213–2222. http://dx.doi.org/10.1016/j.csbj.2021.03.017.

Cowan, A.R., Costanzo, C.M., Benham, R., Loveridge, E.J., Moody, S.C., 2022. Fungal bioremediation of polyethylene: Challenges and perspectives. J. Appl. Microbiol. 132, 78–89. http://dx.doi.org/10.1111/jam.15203.

Cui, H., Zhang, L., Söder, D., Tang, X., Davari, M.D., Schwaneberg, U., 2021. Rapid and oriented immobilization of laccases on electrodes via a methionine-rich peptide. ACS Catal. 11 (4), 2445–2453. http://dx.doi.org/10.1021/acscatal.0c05490.

Eichkorn, K., Weigend, F., Treutler, O., Ahlrichs, R., 1997. Auxiliary basis sets for main row atoms and transition metals and their use to approximate coulomb potentials. Theor. Chem. Acc. 97 (1), 119–124. http://dx.doi.org/10.1007/s002140050244.

Evans, R., O'Neill1, M., Pritzel, A., Antropova, N., Senior, A., Green, T., Žídek, A., Bates, R., Blackwell, S., Yim, J., Ronneberger, O., Bodenstein, S., Zielinski, M., Bridgland, M., Potapenko, A., Cowie, A., Tunyasuvunakool, K., Jain, R., Clancy, E., Kohli, P., Jumper, J., Hassabis, D., 2021. Protein complex prediction with AlphaFold-multimer. http://dx.doi.org/10.1101/2021.10.04.463034, bioRxiv.

Eyheraguibel, B., Traikia, M., Fontanella, S., Sancelme, M., Bonhomme, S., Fromageot, D., Lemaire, J., Lauranson, G., Lacoste, J., Delort, A.M., 2017. Characterization of oxidized oligomers from polyethylene films by mass spectrometry and NMR spectroscopy before and after biodegradation by a *Rhodococcus rhodochrous* strain. Chemosphere 184, 366e374. http://dx.doi.org/10.1016/j.chemosphere.2017.05.137.

Fontanella, S., Bonhomm, S., Koutny, M., Husarova, L., Brusson, J.-M., Courdavault, J.-P., Pitteri, S., Samuel, G., Pichon, G., Lemaire, J., Delort, A.-M., 2010. Comparison of the biodegradability of various polyethylene films containing pro-oxidant additives. Polym. Degrad. Stab. 95 (6), 1011–1021. http://dx.doi.org/10.1016/j.polymdegradstab.2010.03.00.

Fujisawa, M., Hirai, H., Nishida, T., 2001. Degradation of polyethylene and nylon-66 by the laccase-mediator system. J. Polym. Environ. 9, 103–108. http://dx.doi.org/10.1023/A:1020472426516.

Gräff, M., Buchholz, P.C.F., Le Roes-Hill, M., Pleiss, J., 2020. Multicopper oxidases: modular structure, sequence space, and evolutionary relationships. Proteins 88, 1329–1339. http://dx.doi.org/10.1002/prot.25952.

Granja-Travez, R.S., Wilkinson, R.C., Persinoti, G.F., Squina, F.M., Fülöp, V., Bugg, T.D.H., 2018. Structural and functional characterisation of multi-copper oxidase CueO from lignin-degrading bacterium *Ochrobactrum* sp. reveal its activity towards lignin model compounds and lignosulfonate. FEBS J. 285 (9), 1684–1700. http://dx.doi.org/10.1111/febs.14437.

Gravouil, K., Ferru-Clément, R., Colas, S., Helye, R., Kadri, L., Bourdeau, L., Moumen, B., Mercier, A., Ferreira, T., 2017. Transcriptomics and lipidomics of the environmental strain *Rhodococcus ruber* point out consumption pathways and potential metabolic bottlenecks for polyethylene degradation. Environ. Sci. Technol. 51, 5172–5181. http://dx.doi.org/10.1021/acs.est.7b00846.

Grimme, S., Antony, J., Ehrlich, S., Krieg, H., 2010. A consistent and accurate ab initio parametrization of density functional dispersion correction (DFT-D) for the 94 elements H-Pu. J. Chem. Phys. 132 (15), 154104. http://dx.doi.org/10.1063/1.3382344.

Guan, Z.-B., Luo, Q., Wang, H.-R., Chen, Y., Liao, X.R., 2018. Bacterial laccases: Promising biological green tools for industrial applications. Cell Mol. Life Sci. 75 (19), 3569–3592. http://dx.doi.org/10.1007/s00018-018-2883-z.

Janusz, G., Pawlik, A., Świderska-Burek, A., Polak, J., Sulej, J., Jarosz-Wilkołazka, A., Paszczyński, A., 2020. Laccase properties, physiological functions, and evolution. Int. J. Mol. Sci. 21 (3), 966. http://dx.doi.org/10.3390/ijms21030966.

Jones, S.M., Solomon, E.I., 2015. Electron transfer and reaction mechanism of laccases. Cell. Mol. Life Sci. 72 (5), 869–883. http://dx.doi.org/10.1007/s00018-014-1826-6.

Jumper, J., Evans, R., Pritzel, A., Green, T., Figurnov, M., Ronneberger, O., Tunyasuvunakool, K., Bates, R., Žídek, A., Potapenko, A., Bridgland, A., Meyer, C., Kohl, S.A.A., Ballard, A.J., Cowie, A., Romera-Paredes, B., Nikolov, S., Jain, R., Adler, J., Back, T., Petersen, S., Reiman, D., Clancy, E., Zielinski, M., Steinegger, M., Pacholska, M., Berghammer, T., Bodenstein, S., Silver, D., Vinyals, O., Senior, A.W., Kavukcuoglu, K., Kohli, P., Hassabis, D., 2021. Nature 596, 583–589. http://dx.doi.org/10.1038/s41586-021-03819-2.

Kallio, J.P., Auer, S., Jänis, J., Andberg, M., Kruus, K., Rouvinen, J., Koivula, A., Hakulinen, N., 2009. Structure-function studies of a *Melanocarpus albomyces* laccase suggest a pathway for oxidation of phenolic compounds. J. Mol. Biol. 392, 895–909. http://dx.doi.org/10.1016/j.jmb.2009.06.053.

Klamt, A., Schüürmann, G., 1993. COSMO: a new approach to dielectric screening in solvents with explicit expressions for the screening energy and its gradient. J. Chem. Soc. Perkin Trans. 2, 799–805. http://dx.doi.org/10.1039/P29930000799.

Lee, C., Yang, W., Parr, R.G., 1988. Development of the Colle–Salvetti correlation-energy formula into a functional of the electron density. Phys. Rev. B 37 (2), 785–789. http://dx.doi.org/10.1103/physrevb.37.785.

Li, H., Webb, S.P., Ivanic, J., Jensen, J.H., 2004. Determinants of the relative reduction potentials of type-1 copper sites in proteins. J. Am. Chem. Soc. 126 (25), 8010–8019. http://dx.doi.org/10.1021/ja049345y.

Macellaro, G., Baratto, M.C., Piscitelli, A., Pezzella, C., Fabrizi de Biani, F., Palmese, A., Piumi, F., Record, E., Basosi, R., Sannia, G., 2014. Effective mutations in a high redox potential laccase from *Pleurotus ostreatus*. Appl. Microbiol. Biotechnol. 98, 4949–4961. http://dx.doi.org/10.1007/s00253-013-5491-8.

Mangiagalli, M., Carvalho, H., Natalello, A., Ferrario, V., Pennati, M.L., Barbiroli, A., Lotti, M., Pleiss, J., Brocca, S., 2020. Diverse effects of aqueous polar co-solvents on *Candida antarctica* lipase B. Int. J. Biol. Macromol. 150, 930.940. http://dx.doi.org/10.1016/j.ijbiomac.2020.02.145.

Maniatis, T., Fritsch, E.F., Sambrook, J., 1982. Molecular Cloning: A Laboratory Manual. Cold Spring Harbor Laboratory, Cold Spring Harbor, New York.

Mehra, R., Keep, K.P., 2019. Contribution of substrate reorganization energies of electron transfer to laccase activity. Phys. Chem. Chem. Phys. 21 (28), 15805–15814. http://dx.doi.org/10.1039/C9CP01012B.

Mirdita, M., Schütze, K., Moriwaki, Y., Heo, L., Ovchinnikov, S., Steinegger, M., 2021. ColabFold: making protein folding accessible to all. Nature Methods 19, 679–682. http://dx.doi.org/10.1038/s41592-022-01488-1.

Mitchell, A.L., Attwood, T.K., Babbitt, P.C., Blum, M., Bork, P., Bridge, A., Brown, S.D., Chang, H.-Y., El-Gebali, S., Fraser, M.I., Gough, J., Haft, D.R., Huang, H., Letunic, I., Lopez, R., Luciani, A., Madeira, F., Marchler-Bauer, A., Mi, H., Natale, D.A., Necci, M., Nuka, G., Orengo, C., Pandurangan, A.P., Paysan-Lafosse, T., Pesseat, S., Potter, S.C., Qureshi, M.A., Rawlings, N.D., Redaschi, N., Richardson, L.J., Rivoire, C., Salazar, G.A., Sangrador-Vegas, A., Sigrist, C.J.A., Sillitoe, I., Sutton, G.G., Thanki, N., Thomas, P.D., Tosatto, S.C.E., Yong, S.-Y., Finn, R.D., 2019. InterPro in 2019: improving coverage, classification and access to protein sequence annotations. Nucleic Acids Res. 47 (D1), D351–D360.

Montazer, Z., Najafi, M.B.H., Levin, D.B., 2019. Microbial degradation of low-density polyethylene and 2 synthesis of polyhydroxyalkanoate polymers. Can. J. Microbiol. 65, 224–234. http://dx.doi.org/10.1139/cjm-2018-0335.

Montazer, Z., Najafi, M.B.H., Levin, D.B., 2020. Challenges with verifying microbial degradation of polyethylene. Polymers 12, 123. http://dx.doi.org/10.3390/polym12010123.

Nakashima, N., Tamura, T., 2004. A novel system for expressing recombinant proteins over a wide temperature range from 4 to 35 °C. Biotechnol. Bioeng. 86 (2), 136–148. http://dx.doi.org/10.1002/bit.20024.

Pathak, V.M., Navneet, 2017. Review on the current status of polymer degradation: a microbial approach. Bioresour. Bioprocess. 4, 15. http://dx.doi.org/10.1186/s40643-017-0145-9.

Plastics Europe (Ed.), 2019. Plastics - the Facts, 2019 ed. Plastics Europe, https://www.plasticseurope.org/application/files/9715/7129/9584/FINAL_web_version_Plastics_the_facts2019_14102019.pdf. (Accessed 10 March 2022).

Pometto, A.L., Lee, B.T., Johnson, K.E., 1992. Production of an extracellular polyethylene-degrading enzyme(s) by *Streptomyces* species. Appl. Environ. Microbiol. 58, 731–733. http://dx.doi.org/10.1128/aem.58.2.731-733.1992.

Reiss, R., Ihssen, J., Thöny-Meyer, L., 2011. Bacillus pumiluslaccase: a heat stable enzyme with a wide substrate spectrum. BMC Biotechnol. 11, 9. http://dx.doi.org/10.1186/1472-6750-11-9.

Restrepo-Flórez, J.-M., Bassi, A., Thompson, M.R., 2014. Microbial degradation and deterioration of polyethylene - a review. Int. Biodeterioration Biodegrad. 88, 83–90.

Rovaletti, A., De Gioia, L., Fantucci, P., Greco, C., Vertemara, J., Zampella, G., Arrigoni, F., Bertini, L., 2023. Recent theoretical insights into the oxidative degradation of biopolymers and plastics by metalloenzymes. Int. J. Mol. Sci. 24, 6368. http://dx.doi.org/10.3390/ijms24076368.

Sambrook, J., Russell, D.W., 1989. Molecular Cloning: A Laboratory Manual. Cold Spring Harbor Laboratory, Cold Spring Harbor, New York.

Sandt, C., Waeytens, J., Deniset-Besseau, A., Nielsen-Leroux, C., Réjasse, A., 2021. Use and misuse of FTIR spectroscopy for studying the bio-oxidation of plastics. Spectrochim. Acta A 258, 119841. http://dx.doi.org/10.1016/j.saa.2021.119841.

Sanluis-Verdes, A., Colomer-Vidal, P., Rodriguez-Ventura, F., Bello-Villarino, M., Spinola-Amilibia, M., Ruiz-Lopez, E., Illanes-Vicioso, R., Castroviejo, P., Aiese Cigliano, R., Montoya, M., Falabella, P., Pesquera, C., Gonzalez-Legarreta, L., Arias-Palomo, E., Solà, M., Torroba, T., Arias, C.F., Bertocchini, F., 2022. Wax worm saliva and the enzymes therein are the key to polyethylene degradation by *Galleria mellonella*. Nature Commun. 13, 5568. http://dx.doi.org/10.1038/s41467-022-33127-w.

Santo, M., Weitsman, R., Sivan, A., 2013. The role of the copper-binding enzyme - laccase - in the biodegradation of polyethylene by the actinomycete *Rhodococcus ruber*. Int. Biodeterioration Biodegrad. 84, 204–210. http://dx.doi.org/10.1016/j.ibiod.2012.03.001.

Schafer, A., Huber, C., Ahlrichs, R., 1994. Fully optimized contracted Gaussian basis sets of triple zeta valence quality for atoms Li to Kr. J. Chem. Phys. 100 (8), 5829–5835. http://dx.doi.org/10.1063/1.467146.

Serrano-Posada, H., Valderrama, B., Stojanoff, V., Rudiño-Piñera, E., 2011. Thermostable multicopper oxidase from *Thermus thermophilus* HB27: crystallization and preliminary X-ray diffraction analysis of apo and holo forms. Acta Crystallogr. F 67, 1595–1598. http://dx.doi.org/10.1107/S174430911103805X.

Solomon, E.I., Heppner, D.E., Johnston, E.M., Ginsbach, J.W., Cirera, J., Qayyum, M., Kieber-Emmons, M.T., Kjaergaard, C.H., Hadt, R.G., Tian, L., 2014. Copper active sites in biology. Chem. Rev. 114 (7), 3659–3853. http://dx.doi.org/10.1021/cr400327t.

Sowmya, H.V., Ramalingappa, M.K., Thippeswamy, B., 2014. Degradation of polyethylene by *Trichoderma harzianum*-SEM, FTIR, and NMR analyses. Environ. Monit. Assess. 186, 6577–6586. http://dx.doi.org/10.1007/s10661-014-3875-6.

Sowmya, H.V., Ramalingappa, M.K., Thippeswamy, B., 2015. Degradation of polyethylene by *Penicillium simplicissimum* isolated from local dumpsite of Shivamogga district. Environ. Dev. Sustain. 17 (4), 731–745. http://dx.doi.org/10.1007/s10668-014-9571-4.

Thompson, J.D., Higgins, D.G., Gibson, T.J., 1994. CLUSTAL W: improving the sensitivity of progressive multiple sequence alignment through sequence weighting, position-specific gap penalties and weight matrix choice. Nucleic Acids Res. 22 (22), 4673–4680. http://dx.doi.org/10.1093/nar/22.22.4673.

Trubitzina, L.I., Abdullatypov, A.V., Larionova, A.P., Trubitsin, I.V., Alferov, S.V., Ponamoreva, O.N., Leontievsky, A.A., 2021. Expression of thermophilic two-domain laccase from *Catenuloplanes japonicus* in *Escherichia coli* and its activity against triarylmethane and azo dyes. Peer J. 9, e11646.

Wei, R., Zimmermann, W., 2017. Microbial enzymes for the recycling of recalcitrant petroleum-based plastics: how far are we? Microb. Biotechnol. 10, 1308–1322. http://dx.doi.org/10.1111/1751-7915.12710.

Xu, P., Du, H., Peng, X., Tang, Y., Zhou, Y., Chen, X., Fei, J., Meng, Y., Yuan, L., 2020. Degradation of several polycyclic aromatic hydrocarbons by laccase in reverse micelle system. Sci. Total Environ. 708, http://dx.doi.org/10.1016/j.scitotenv.2019.134970, 708:134970.

Xu, F., Shin, W., Brown, S.H., Wahleithner, J.A., Sundaram, U.M., Solomon, E.I., 1996. A study of a series of recombinant fungal laccases and bilirubin oxidase that exhibit significant differences in redox potential, substrate specificity, and stability. B. B. A. Prot. St. 1292 (2), 303–311. http://dx.doi.org/10.1016/0167-4838(95)00210-3.

Yao, C., Xia, W., Dou, M., Du, Y., Wu, J., 2022. Oxidative degradation of UV-irradiated polyethylene by laccase-mediator system. J. Hazard. Mater. 440, 129709. http://dx.doi.org/10.1016/j.jhazmat.2022.129709.

Yeung, C.W.S., Teo, J.Y.Q., Loh, X.J., Lim, J.Y.C., 2021. Polyolefins and polystyrene as chemical resources for a sustainable future: challenges, advances, and prospects. ACS Mater. Lett. 3 (12), 1660–1676. http://dx.doi.org/10.1021/acsmaterialslett.1c00490.

Zampolli, J., Collina, E., Lasagni, M., Di Gennaro, P., 2014. Biodegradation of variable-chain-length *n*-alkanes in *Rhodococcus opacus* R7 and the involvement of an alkane hydroxylase system in the metabolism. AMB Express 4, 73. http://dx.doi.org/10.1186/s13568-014-0073-4.

Zampolli, J., Di Canito, A., Cappelletti, M., Collina, E., Lasagni, M., Di Gennaro, P., 2020. Biodegradation of naphthenic acids: identification of *Rhodococcus opacus* R7 genes as molecular markers for environmental monitoring and their application in slurry microcosms. Appl. Microbiol. Biotechnol. 104, 2675–2689. http://dx.doi.org/10.1007/s00253-020-10378-5.

Zampolli, J., Orro, A., Manconi, A., Ami, D., Natalello, A., Di Gennaro, P., 2021. Transcriptomic analysis of *Rhodococcus opacus* R7 grown on polyethylene by RNA-seq. Sci. Rep. 11, 21311. http://dx.doi.org/10.1038/s41598-021-00525-x.

Zampolli, J., Orro, A., Vezzini, D., Di Gennaro, P., 2022. Genome-based exploration of *Rhodococcus* species for plastic-degrading genetic determinants using bioinformatic analysis. Microorganisms 10, 1846. http://dx.doi.org/10.3390/microorganisms10091846.

Zampolli, J., Zeaiter, Z., Di Canito, A., Di Gennaro, P., 2018. Genome analysis and -omics approaches provide new insights into the biodegradation potential of *Rhodococcus*. Appl. Microbiol. Biotechnol. 103, 1069–1080. http://dx.doi.org/10.1007/s00253-018-9539-7.

Zeng, J., Lin, X., Zhang, J., Li, X., Wong, M.H., 2011. Oxidation of polycyclic aromatic hydrocarbons by the bacterial laccase CueO from *E. coli*. Appl. Microbiol. Biotechnol. 89 (6), 1841–1849. http://dx.doi.org/10.1007/s00253-010-3009-1.

Zhang, A., Hou, Y., Wang, Q., Wang, Y., 2022a. Characteristics and polyethylene biodegradation function of a novel cold-adapted bacterial laccase from Antarctic sea ice psychrophile *Psychrobacter* sp. NJ228. J. Hazard. Mater. 439, 129656. http://dx.doi.org/10.1016/j.jhazmat.2022.129656.

Zhang, Y., Pedersen, J.N., Eser, B.E., Guo, Z., 2022b. Biodegradation of polyethylene and polystyrene: From microbial deterioration to enzyme discovery. Biotechnol. Adv. 60, 107991. http://dx.doi.org/10.1016/j.biotechadv.2022.107991.

Zhang, F., Zhao, Y., Wang, D., Yan, M., Zhang, J., Zhang, P., Ding, T., Chen, L., Chen, C., 2021. Current technologies for plastic waste treatment: a review. J. Clean. Prod. 282, 124523. http://dx.doi.org/10.1016/j.jclepro.2020.124523.